Unified Particle System for Multiple-fluid Flow and Porous Material

BO REN*, Nankai University, China
BEN XU*, Nankai University, China
CHENFENG LI, Swansea University, UK

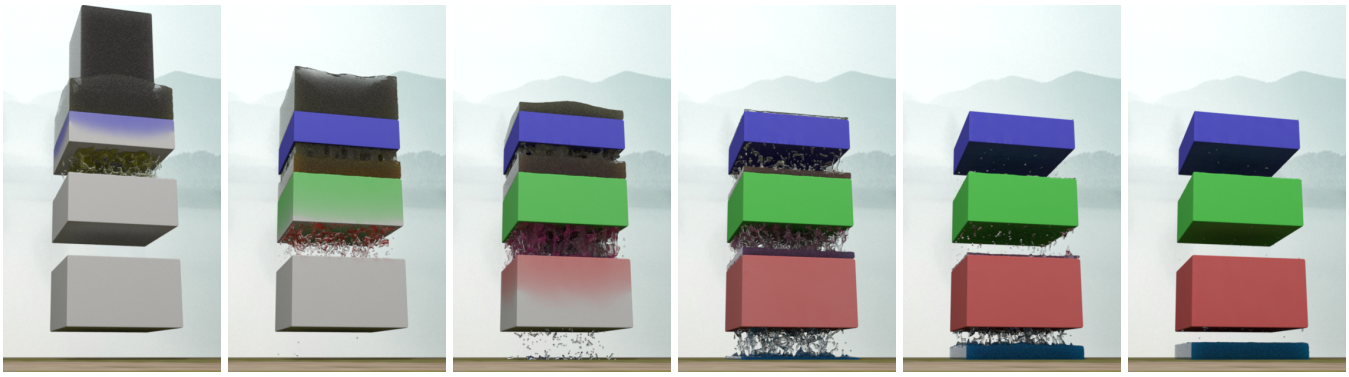

Fig. 1. Selective filtering of a three-phase liquid mixture. The black liquid mixture flows through a vertical filter consisting of three layers of foam, each absorbing one fluid phase (red, green or blue). The porous foams turn into different colours as the mixture is selectively filtered.

Porous materials are common in daily life. They include granular material (e.g. sand) that behaves like liquid flow when mixed with fluid and foam material (e.g. sponge) that deforms like solid when interacting with liquid. The underlying physics is further complicated when multiple fluids interact with porous materials involving coupling between rigid and fluid bodies, which may follow different physics models such as the Darcy's law and the multiple-fluid Navier-Stokes equations. We propose a unified particle framework for the simulation of multiple-fluid flows and porous materials. A novel virtual phase concept is introduced to avoid explicit particle state tracking and runtime particle deletion/insertion. Our unified model is flexible and stable to cope with multiple fluid interacting with porous materials, and it can ensure consistent mass and momentum transport over the whole simulation space.

CCS Concepts: • **Computing methodologies** → **Physical simulation**.

Additional Key Words and Phrases: porous media, fluid simulation, smoothed particle hydrodynamics, virtual phase

*Both authors contributed equally to the paper

Authors' addresses: Bo Ren, Nankai University, 38 Tongyan Rd, Tianjin, 300350, China, rb@nankai.edu.cn; Ben Xu, Nankai University, 38 Tongyan Rd, Tianjin, 300350, China, xuben@mail.nankai.edu.cn; Chenfeng Li, Swansea University, Energy Safety Research Institute, Bay Campus, Swansea, UK, c.f.li@swansea.ac.uk.

0730-0301/2021/8-ART118 $15.00
https://doi.org/10.1145/3450626.3459764

ACM Reference Format:
Bo Ren, Ben Xu, and Chenfeng Li. 2021. Unified Particle System for Multiple-fluid Flow and Porous Material. *ACM Trans. Graph.* 40, 4, Article 118 (August 2021), 14 pages. https://doi.org/10.1145/3450626.3459764

1 INTRODUCTION

Unlike impermeable materials that can only interact with fluid flows via their surfaces, porous materials present a much stronger coupling when exposed to fluids, and the solid-fluid interaction takes place both on their surfaces and inside their bodies. Phenomena such as water spilling out of a squeezed sponge, sea wave splashing on a sandy beach and cotton toy deforming when wetted are some common examples of fluid flow interacting with porous media. These flow phenomena are far more complicated than the single-phase fluid flow in an open space, and they could involve many physical processes occurring simultaneously, such as liquid mass transport in the porous solid, absorption and emission on the solid surface, hydrophobic and hydrophilic behaviours, capillary effects and multiphase flows.

Simulations of single-fluid flow involving porous materials have been achieved using SPH (smoothed particle hydrodynamics) [Lenaerts et al. 2008] and MPM (material point method) [Tampubolon et al. 2017], producing impressive visual results. Despite the success, both methods face challenges associated with porous behaviours. Using SPH, [Lenaerts et al. 2008] modelled the absorption and emission of liquid by deleting/inserting fluid particles and tracking the fluid flow inside the solid particles. Thus, the simulator must constantly delete/insert non-uniform SPH particles, which needs to be taken extra care of in calculation and implementation. A naive

extension of this approach to multiple fluid simulation will involve splitting the fluid particles, since different fluid phase can potentially interact with the solid differently. This will be an exhausting process producing many fragmented particles. Alternatively, without splitting the fluid particle, one needs to cope with different mass and momentum transports among various phases and maintain consistency for fluid particles crossing the solid boundary. The MPM approach [Tampubolon et al. 2017] uses two layers of grid to model sand and liquid motions separately. For the sand-like porous material, a similar set of Navier-Stokes equations applies both to the pure liquid phase and the solid-liquid mixture so that the focus is on the interaction between these two grid layers. However for other porous materials like sponge, the fluid motions inside and outside the porous solid can differ greatly (the flow in porous media obeys the Darcy's law), and other physical processes like capillary effects may also be involved. Thus, it is not a trivial task to extend the capacity of the multi-grid MPM approach for generic porous media interacting with multiple fluids.

In this paper we present a universal SPH-based simulation scheme for multiple-fluid flows in porous materials. A special emphasis is on sponge-like materials where the internal flow follows Darcy's law and external flow is governed by the Navier-Stokes equations. In our approach, the internal and external flows are modelled uniformly using the volume fraction and a mixture model, avoiding constant particle deletion and insertion. The new approach is able to capture a wide range of porous media flow phenomena, including poroelasticity, capillary effects and variable absorption in multiple-fluid environment. Our main contributions are:

- A universal SPH framework for the simulation of multiple-fluid flow and sponge-like porous materials.
- A novel concept of virtual phase to consistently capture the fluid flow when crossing porous surface and avoid runtime particle deletion/insertion.
- A flexible constitutive modelling strategy based on the virtual phase concept, to support multiple fluid flow, porous material deformation and the coupled physics between fluid and porous solids.

The rest of paper is arranged as follows. Related works are briefly recapped in §2, after which the fundamental theories of our multiple-fluid SPH-based porous model is introduced in §3. We explain our choice of constitutive models in §4, and the designation of SPH discretization in §5. The simulation framework and implementation issues are explained in §6. A number of examples with different visual effects are presented in §7 to demonstrate the performance of our model. Finally, concluding remarks and limitations are discussed in §8.

2 RELATED WORK

2.1 Simulation of Porous Phenomena

Explorations of porous behaviours are studied in a wide range of graphics works involving cloth, sand or mud, and volumetric solid. Some early research works focus on the absorption and diffusion of liquid into solid. [Rungjiratananon et al. 2008] modelled the absorption of water into sand using a combined SPH and DEM (discrete element method) framework, which captures the cohesion change during sand wetting. [Huber et al. 2011] used Fick's law to model liquid diffusion inside wet cloth. Surface flow, absorption and in-cloth diffusion were combined to simulate thin-shell wetting in [Um et al. 2013], where changes of material properties due to wetting are considered.

More complex porous behaviours are also studied in the literature. In [Lenaerts et al. 2008], an SPH-based simulator was proposed for simulating liquid flow in porous materials, where the Darcy flux is introduced to model the absorbed flow behaviour. Their method can be applied to a variety of scenarios involving porous media flow, but requires frequent particle deletion and insertion at solid surface. Later [Lenaerts and Dutre 2009] extended this model for wetted flows of granular materials, and [Lin 2015] combined it with two-way fluid-hair interactions. Fluid-hair interaction including liquid capture and dripping was also studied in [Fei et al. 2017] using a dimension-reduced model for thin liquid on hair cluster. In [Patkar and Chaudhuri 2013], absorbed liquid is stored on a triangle mesh for cloth or a tetrahedral mesh for volumetric solid and a diffusion equation is solved on the mesh structure. They also handled absorption and dripping by a particle absorption and generating scheme with an integrated SPH simulator for liquid flow outside the solid region. Recently, [Fei et al. 2018] used a set of saturated continuity equations for porous flow inside fabric porous materials, which supports anisotropic fabric microstructure and its nonlinear drag and pore pressure forces. Similarly, an integrated bulk liquid simulator is used in their work and a particle absorbing and generating scheme is designed for liquid capturing and dripping. In [Zheng et al. 2020] miscible and immiscible diffusion models are considered to simulate multi-solvent stains on textile. [Ding et al. 2019] combined liquid diffusion and gas stress in a thermomechanical porous model for baking and cooking effect simulation.

As a special case of porous media flow, the granular flow has been receiving increasing attention from the graphics community in recent years. [Baek et al. 2015] classified mud particles into different sizes and solved respective suspension particle motion for muddy flows. [Yan et al. 2016; Yang et al. 2017] used the volume fraction to describe the concentration of granular material in the liquid, and the porous behaviour was treated similarly to solid dissolving. [Gao et al. 2018; Tampubolon et al. 2017] used MPM to simulate granular sand flows in water, and two background grids were used for the fluid and sand phase separately, with the interaction between phases handled through a momentum exchange term. This approach can handle large scenarios effectively, but does not cover wider physics, e.g. capillary phenomena. In addition, the previous research works of granular materials usually use Navier-Stokes equations for both the pure liquid phase and the solid-liquid mixture, while the internal flow could be better captured by using Darcy's law in a general porous medium.

Our approach does not require the physics laws to be the same inside and outside the solid, and at the same time does not need to frequently delete and generate particles at solid surface.

Porous have been studied using different models and theories in relevant fields. Some approaches explicitly model the detailed geometry of porous materials [Berrone et al. 2017; Hilfer 2006; Wu et al. 2004], where a porous material is treated as a network of connected pore spaces and the fluid flow in the pore-space network is tracked by carefully calculating the interactions between pore surface and fluid. In [Jin et al. 2017] porous permeability was modelled by the fractal properties of the porous media. We refer to [Fei et al. 2018] for a more comprehensive summary on modelling approaches of porous media.

2.2 SPH method.

We have integrated our models with the SPH method [Becker and Teschner 2007a; Monaghan 1994; Müller et al. 2003] to establish a unified particle system for multiple-fluid flow and porous material. Thus, in order to place the present work in the right research context, the most relevant research works on SPH are also briefly recapped here. [Aly and Raizah 2018; Ihmsen et al. 2014a] developed pressure projection schemes are developed for SPH fluid simulation, and [Bender and Koschier 2016; Macklin and Müller 2013; Solenthaler and Pajarola 2009] ensured the incompressibility by prediction-correction schemes. Solid-fluid boundary coupling is also comprehensively studied in the SPH literature. By sampling the solid surface with particles, [Akinci et al. 2012] proposed a versatile rigid-fluid coupling method. In [Band et al. 2018a], by integrating with the implicit incompressible SPH (IISPH), better boundary particle pressure calculation that ensures physically meaningful pressure gradient was achieved. Recently, [Band et al. 2018b] adopted a moving least square technique to further reduce false velocity artifacts at the boundary. On the other hand, stability issues were also studied using density maps [Bender et al. 2020; Koschier and Bender 2017] or an interleaved velocity update iterative solver [Gissler et al. 2019]. The above incompressibility and solid-liquid coupling studies are all for single-fluid flow and the discussion on miscible multiple fluids is sparse. For other SPH research topics, we refer to [Ihmsen et al. 2014b] and [Koschier et al. 2019], which provide thorough surveys of the graphics SPH literature.

2.3 Multiple fluid simulation.

The multiple fluid simulation has been studied by the graphics community for over a decade. Several grid-based simulators were developed for interfacial flow [Hong and Kim 2005; Kim 2010; Losasso et al. 2006], where the interfaces between different phases are exactly tracked. Volume fraction based grid solvers were proposed in [Bao et al. 2010; Kang et al. 2010], where miscible phases are simulated. [Nielsen and Osterby 2013] solved the full two-fluid Navier-stokes equations implicitly providing vivid visual appearance of water sprays. The volume fraction concept has been widely adopted in recent particle-based frameworks. SPH-based mixture-model multiple-fluid simulator was proposed by [Ren et al. 2014; Yan et al. 2016] where a phase-wise drift velocity is essential for various mixing/unmixing effects in multiple-fluid flow including solid. By combining Navier-Stokes equation with a phase-field model, [Yang et al. 2017, 2015] proposed an energy-based multiple fluid solver that also captures distillation effects. The material point method (MPM) has shown its effectiveness in multiple fluid simulations as well. [Yan et al. 2018] proposed a MPM-based multiple fluid solver to model interactions between multiple fluid and solid phases. [Gao et al. 2018; Tampubolon et al. 2017] targeted granular flows using a two-layer grid for solid and liquid phases. In all these studies, the solid phase is either impermeable or follows the same fluid governing equations after dissolving. To simulate sponge-like materials, our work allows flows inside and outside the solid to follow different physics laws.

Fluid mixture simulations are also studied in many other works such as in surface flows [Ren et al. 2018b] and viscosity blending model for shear thinning fluids [Nagasawa et al. 2019]. We refer to [Ren et al. 2018a] for a more comprehensive summary of graphics multiple-fluid studies.

3 UNIVERSAL SPH MODEL FOR MULTIPHASE FLOW AND POROUS MATERIAL

3.1 Problem Formulation

A simulation space involving porous materials and fluid flows can be naturally divided into two parts, i.e. the "inner" and "outer" regions of the porous material, and the fluid flow travels in or between these two regions. In our universal SPH model, we consider a general case where there are three coupled physical mechanisms, i.e. porous solid motion, inner fluid transport, and outer fluid motion, and they may follow different physical laws. Therefore, we consider three sets of governing equations that describes each of the three parts in the coupled physics of multiple-fluid flow and porous materials.

First, for fluid flow inside the porous material, we use Darcy's law [Darcy 1856] to simulate the flow motion. Specifically, the instantaneous flow rate, i.e. Darcy flux, in a homogeneous permeable material is determined by

$$\mathbf{q}_k = -\frac{\mathbf{k}_{wk}}{\mu_k} \cdot \nabla p_s^{pore}, \tag{1}$$

where the subscript k denotes the k-th fluid phase, $\mathbf{q}_k$ Darcy flux of the phase k, $\mathbf{k}_{wk}$ the permeability tensor, μ_k the fluid viscosity, and the pore pressure p^{pore} represents the pressure of fluid in the pore space. Based on experiments and the homogenization of Navier-Stokes equations, the Darcy's law describes porous flow in porous solids. The pore pressure in Darcy's law is determined by the states of solid and locally absorbed fluid, and represented by Eq. (1) it drives the absorbed fluid from the region with pore pressure to the region with low pore pressure.

Next, for fluid flow outside the porous material, we adopt the multiple-fluid mixture model [Ren et al. 2014; Yan et al.

2016]:

$$\frac{D\tilde{\alpha}_k}{Dt} = -\tilde{\alpha}_k \nabla \cdot \mathbf{u}_m - \nabla \cdot (\tilde{\alpha}_k \tilde{\mathbf{u}}_{mk}) \tag{2}$$

$$\frac{\partial}{\partial t}\mathbf{u}_m + (\mathbf{u}_m \cdot \nabla)\mathbf{u}_m = \mathbf{g} + \mathbf{a}^{press} + \mathbf{a}^{other}, \tag{3}$$

where $\tilde{\alpha}_k$ is the volume fraction of phase k, $\mathbf{u}_m$ and $\tilde{\mathbf{u}}_{mk}$ are the mixture velocity and drift velocity of the phase k, and $\mathbf{g}$, $\mathbf{a}^{press}$ and $\mathbf{a}^{other}$ denote the gravity, pressure, and other influencing factors (viscosity, etc.), respectively. We use the tilde notation in the above equations to distinguish them from the "virtual-phase" quantities we are going to introduce. The mixture model expresses the continuity and momentum equations through aggregate values averaged over the local volume, which for SPH is the particle. It can capture the phase-wise velocity difference, but only needs to solve for the particle velocity by analytically computing the drift velocities. In the mixture model solver, standard particle advance scheme can be used and the phase volume fraction changes within a particle is automatically handled by the continuity equation.

Finally, for the porous solid, we adopt the elastic solid model [Peer et al. 2018] which is a corotated material model. The strain tensor ϵ is expressed as:

$$\epsilon = \frac{1}{2}(\mathbf{F} + \mathbf{F}^T) - \mathbf{I}, \tag{4}$$

where $\mathbf{F}$ is the deformation gradient tensor and $\mathbf{I}$ is the identity matrix. To take into account the effect of pore pressure on the deformation of solid and inspired by [Lenaerts et al. 2008], we add a term $-\eta p^{pore}\mathbf{I}$ to their stress tensor and express the stress tensor $\mathbf{P}$ as follows:

$$\mathbf{P} = 2\nu\epsilon + \lambda \mathrm{tr}(\epsilon)\mathbf{I} - \eta p_s^{pore}\mathbf{I}, \tag{5}$$

where ν, λ are Lamé parameters and η is a solid constant. The last term was introduced in [Lenaerts et al. 2008] and represents the effect of pore pressure, i.e. absorbing fluid will let the solid expand.

In our study, the above governing equations are discretized using two kinds of particles, i.e. solid particles representing the porous solid and fluid particles representing fluid flow. A discretization problem emerges from the inner/outer fluid coupling, i.e. transition between outer and inner fluids. Previous approaches [Fei et al. 2018; Lenaerts et al. 2008; Patkar and Chaudhuri 2013] typically use different solvers for inner and outer regions, with the SPH particles representing the fluid placed only in the outer region. As a result, SPH particles are deleted or inserted when fluid passes through the surface of porous material. This method becomes exhausting for multiple fluid simulation when different fluid phases interact with the porous solid in different ways, producing many particles with non-uniform sizes near the porous solid interface. On the contrary, we design our approach to let fluid particles remain in the simulation when they cross the surface of porous material (whether through absorbing or emitting). No particle gets deleted or inserted at interface crossing. This is achieved by a novel extension of the volume fraction representation and the mixture model [Ren et al. 2014], which in turn leads to a universal simulation framework. More details are explained in §3.2.

3.2 Virtual Phase for Fluid Particles

The above governing equations can be solved individually with existing methods, but they become strongly coupled near the surface of porous material, greatly increasing the solution complexity. We propose the concept of virtual phase to handle the state change of fluid particles crossing the interface and the associated mass and momentum transport in a uniform manner, thereby avoiding explicit state tracking and runtime particle deletion/insertion.

Specifically, we assign each fluid particle with two virtual phases α_k and β_k, which represent the volume fractions of the phase k in the outer and inner regions, respectively, and they satisfy the relation $\sum_k (\alpha_k + \beta_k) = 1$. Thus, $\sum_k \alpha_k = 1$ indicates that the fluid particle locates outside the porous material, $\sum_k \beta_k = 1$ indicates that the particle locates inside the porous material, and non-zero α and β values indicate that the fluid particle is near the surface of porous material. Consider an example where a fluid particle at a two-phase state is moving from the outer region into the inner region, but only one fluid phase can be absorbed into the porous material while the other cannot. The mass transport, momentum and position change of this fluid particle are affected by all material phases, each in turn may have separate inner and outer fractions following different laws in the inner and outer regions. The virtual phase concept distinguishes these fractions and virtual phases can follow separate governing equations. The virtual phases have a property that α_k and β_k can be transferred, by absorption or other mechanisms, near the surface of porous material without violating the mass conservation law, but volume fractions between real phases cannot be simply transferred.

Aided by the virtual fraction concept, the inner and outer fluid particle dynamics can be solved in a universal manner using an extended mixture model. The complex inner-outer state transition under different phase behaviour in relation to the porous solid is then handled by solving continuity equations in the multiple-fluid model. The universal equations for all fluid particles are:

$$\frac{D\alpha_k}{Dt} = -\alpha_k \nabla \cdot \mathbf{u}_m - \nabla \cdot (\alpha_k \mathbf{u}_{mk,\alpha}) + \nabla \cdot \mathbf{D_k} \tag{6}$$

$$\frac{D\beta_k}{Dt} = -\beta_k \nabla \cdot \mathbf{u}_m - \nabla \cdot (\beta_k \mathbf{u}_{mk,\beta}) - \nabla \cdot \mathbf{D_k} \tag{7}$$

$$\frac{\partial}{\partial t}\mathbf{u}_m + (\mathbf{u}_m \cdot \nabla)\mathbf{u}_m = \mathbf{g} + \mathbf{a}^{press} + \mathbf{a}^{pore} + \mathbf{a}^{cap} + \mathbf{a}^{other}, \tag{8}$$

where α_k and β_k are the outer and inner volume fractions of phase k, $\mathbf{u}_m$ and $\mathbf{u}_{mk,\alpha}, \mathbf{u}_{mk,\beta}$ are the fluid-particle velocity and drift velocity of the outer and inner fluids, $\mathbf{D}_k$ is the absorption flux and $\nabla \cdot \mathbf{D}_k$ is an absorption source term, and $\mathbf{g}$, $\mathbf{a}^{press}$, $\mathbf{a}^{pore}$, $\mathbf{a}^{cap}$, $\mathbf{a}^{other}$ denote the accelerations from gravity, pressure, pore pressure, capillary forces and other factors (e.g. viscosity), respectively.

This extended mixture model can simulate the fluid particles in a universal manner and handle the coupling between the governing equations described in §3.1. Eq. (6) and Eq. (7) are the continuity equations, where the outer and inner fluids are separately calculated since the different mass transportation laws they follow lead to different $\mathbf{u}_{mk}$ whose calculations will be described in detail later. A pure inner fluid particle will only be affected by $\mathbf{a}^{pore}$, which links the Darcy's law with the elastic solid model. A pure outer fluid particle will have zero $\mathbf{a}^{pore}$ term, but then the solid particles can provide boundary pressures in $\mathbf{a}^{press}$ for solving outer-region fluid motion. For a hybrid particle near the solid surface, those terms can all be non-zero. A demonstration on the coupling relations of the governing equations is shown in Fig. 2, and more details will be given in the later sections.

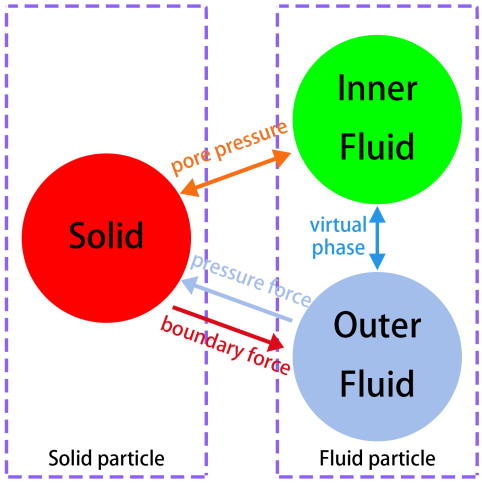

Fig. 2. The coupling between multiple fluids and porous solid. The governing equations for solid, inner fluid and outer fluid are represented by the red, green and blue disks, respectively, and the arrows between them indicate the physical interactions involved in the coupling.

4 CONSTITUTIVE MODELS

In our framework, the solid and fluids are described by Eqs.(4,5) and Eqs.(6,7,8), respectively, where a range of constitutive models are required. They include the pore pressure, drift velocities, and absorption and capillary effects, which are explained in detail in § 4.1, § 4.2 and § 4.3, respectively.

4.1 Pore pressure

The key factors for the solid and fluid momentum balance in the inner region are the pore pressure and the Darcy flux. Pore pressure raises when there are more absorbed fluid or the solid get squeezed, while the Darcy flux is proportional to its gradient using Eq. (1). Based on the theory of poroelasticity [Detournay and Cheng 1993], the pore pressure in the solid is obtained by

$$p_s^{pore} = p_0 \sum_k \phi_{sk} - B\mathrm{tr}(\epsilon), \tag{9}$$

where p_0 is the rest pore pressure, $\mathrm{tr}(\epsilon)$ the volumetric strain, B a Biot's ratio constant determined by the Biot's modulus and the Biot's coefficient of the solid, and ϕ_{sk} the phase k's absorbed volume rate (see § 5 for details). The above pore pressure is computed on the solid particles and can be directly used for solid motion computations. We then compute its gradient on fluid particles for the Darcy flux in Eq. (1) by collecting nearby solid particle information.

The pore pressure affects the behaviour of solid as described in Eq. (5), and it is also a driving force for the fluid flow inside solid. A pore pressure is exerted to the internal fluid and if no other forces are present, its contribution ends at the next simulation step, making the relative fluid-solid velocity $\mathbf{u}_{rk}$ agree with the Darcy flux in Eq. (1) through $\mathbf{u}_{rk} = \mathbf{q}_k/e$, where e is called porosity describing the fraction of void volume over the total volume. We thus add a term $\mathbf{a}^{pore}$ in Eq. (8) to model this force source in the simulation of inner and outer fluid. Specifically, we use

$$\mathbf{a}^{pore} = \sum_k \frac{\beta_k}{\rho_{fm}\Delta t}(\rho_k \mathbf{u}_{\beta k} - \rho_{\beta m}\mathbf{u}_m), \tag{10}$$

where $\rho_{\beta m} = \sum_k \frac{\beta_k \rho_k}{\sum_{k'} \beta_{k'}}$ is the inner rest density, $\mathbf{u}_{\beta k} = \mathbf{u}_{rk} + \mathbf{u}_s$ is the world-coordinate phase velocity of phase k, $\mathbf{u}_s$ is the solid velocity, $\rho_{fm} = \sum_k (\alpha_k + \beta_k)\rho_k$ is the aggregate density of fluid particle. The derivation is provided in Appendix B.

4.2 Drift Velocities

The drift velocity represents the relative velocity between the local phase and the aggregate mixture particle, and it plays a key role in capturing the multiple fluid behaviours in the mixture model [Ren et al. 2014; Yan et al. 2016]. By taking into account the drift velocity in the continuity equation, the mixture model can automatically handle the volume fraction changes of each phase within a particle during bulk flow motion. This feature is beneficial to our problem in that the virtual phase volume fractions can be similarly solved by Eqs.(6,7) without explicitly distinguishing inner or outer fluid particles in solving the bulk fluid motion.

We extend the drift velocity from [Ren et al. 2014; Yan et al. 2016] to cope with the porous fluid simulation. For an outer fluid virtual phase α_k, its drift velocity is:

$$\begin{aligned}\mathbf{u}_{mk,\alpha} =& \tau(\rho_k - \sum_{k'} c_{\alpha k'}\rho_{k'})\mathbf{a} - \tau(\nabla p_k - \sum_{k'} c_{\alpha k'}\nabla p_{k'}) - \\ & \sigma(\frac{\nabla \alpha_k}{\alpha_k} - \sum_{k'} c_{\alpha k'}\frac{\nabla \alpha_{k'}}{\alpha_{k'}}) - \varphi(\nabla p_k^{pore} - \sum_{k'} c_{\alpha k'}\nabla p_{k'}^{pore}),\end{aligned} \tag{11}$$

where $c_{\alpha k} = \frac{\alpha_k \rho_k}{\sum_{k'} \alpha_{k'}\rho_{\alpha m}}$ denotes the outer mass fraction, $\rho_{\alpha m} = \sum_k \frac{\alpha_k \rho_k}{\sum_{k'} \alpha_{k'}}$ denotes the outer mixture density, $\mathbf{a} = g - (\mathbf{u}_m \cdot \nabla)\mathbf{u}_m - \frac{\partial \mathbf{u}_m}{\partial t}$, and τ, σ and φ are constant weight factors, ∇p_k^{pore} is the gradient of pore pressure of the liquids, which can be phase-specific since different phases usually are absorbed differently. Eq. (11) differs from the original drift velocity only by the last term, which models the sucking or propelling effects due to absorption or emission near

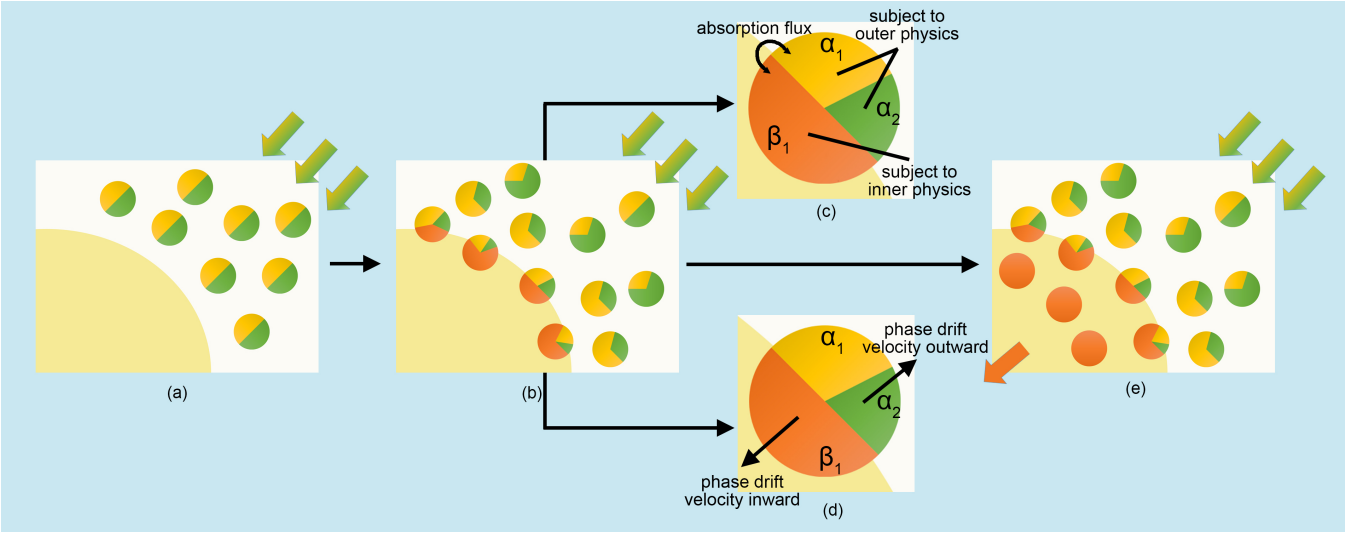

Fig. 3. Particle behavior on solid-liquid boundaries. (a) A two-phase liquid reaches the surface of a porous solid, the yellow phase is absorbable and the green phase is non-absorbable. (b)(c)(d) The absorption flux first transfers the yellow phase to its virtual orange phase, which in turn is subject to the Darcy flux trying to drag the particle inside. Different drift velocities are produced among the virtual phases within a liquid particle. (e) The absorbed particles will be left with more absorbed phase as it goes deeper, and the non-absorbed-phase volume fractions are transferred to the outer-region particles.

the porous solid surface. The calculation of ∇p_k^{pore} will be explained in more details in §4.3 and §5.

The inner fluid virtual phase β_k obeys the Darcy's law within the porous solid, and it does not have the same hydrodynamic pressure as in the outer region. As the pore pressure in the inner region plays the same role as the hydrodynamic pressure of fluids in the outer region, we replace the second term of the original drift velocity equation to form our inner-fluid drift velocity model:

$$\begin{aligned}\mathbf{u}_{mk,\beta} =&\tau(\rho_k - \sum_{k'} c_{\beta k'}\rho_{k'})\mathbf{a} - \tau'(\mathbf{q}_k - \sum_{k'} c_{\beta k'}\mathbf{q}_{k'}) - \\ &\sigma'(\frac{\nabla\beta_k}{\beta_k} - \sum_{k'} c_{\beta k'}\frac{\nabla\beta_{k'}}{\beta_{k'}}),\end{aligned} \tag{12}$$

where $c_{\beta k}$ denote the inner mass fraction (corresponding to $c_{\alpha k}$ defined in Eq. (11)), and τ', σ' are constant weight factors (the apostrophe indicates that they may differ from those in Eq. (11) due to different environment settings of inner and outer regions). Note that it does not matter in Eq. (12) whether $\mathbf{q}_k$ is computed from Eq. (1) (i.e. in the local solid coordinate) or in the world coordinate. As long as the solid porosity is homogeneous, since $\sum_k c_{\beta k} = 1$, we can obtain the same result using $\mathbf{q}_k$ calculated under either coordinate.

4.3 Absorption and Capillary Effects

Fluid absorption and emission can occur between fluid and porous solid. To capture these effects, we assume that the outer fluid also has a phase-wise constant pore pressure p_{0k} that corresponds to different absorption tendencies. When the outer pore pressure is greater than the inner pore pressure, the fluid will get absorbed and a liquid particle may flow into the solid, and vice versa. On the other hand, inside the porous solid, we take a simplification and assume the pore pressure is unified across phases and related to the absorbed fluid volume and volumetric strain by Eq. (9).

Similar to the Darcy flux calculation in Eq. (1), we compute the gradient of pore pressure to obtain the absorption flux:

$$\mathbf{D}_k = -K\frac{\mathbf{k_{wk}}}{\mu_k}(\alpha_k + \phi_{sk})\nabla p_k^{pore}, \tag{13}$$

where K is a constant absorption ratio coefficient related to the solid. The dimensionless term $(\alpha_k + \phi_{sk})$ is multiplied to avoid creating fake flux. Then, Eq. (7) and Eq. (6) are used to determine the exchange of internal and external fluids.

When a part of fluid mass is absorbed by the solid, the fluid particle will be subject to capillary force near the solid surface, preventing liquid escaping from the porous solid. We use a similar model as [Becker and Teschner 2007b] to capture the acceleration due to capillary force:

$$\mathbf{a}^{cap} = \psi\sum_k \beta_k \mathbf{n}, \tag{14}$$

where ψ is a constant strength factor, $\mathbf{n}$ is a normal vector in the direction from a fluid particle to porous solid interior. Near the porous surface, the capillary force generates an inward dragging effect. After the particle flows into the solid, it will gradually reduce to zero so that the motion of fluid particles gets purely governed by the Darcy's law.

4.4 Particle Behavior on Solid-liquid Boundaries

In this subsection we discuss how the coupling mechanisms in Fig. 2 act on a fluid particle near the solid boundary in our simulation framework. In Fig. 3 we use a simple setting to demonstrate how phases within liquid particles change near the solid boundary when they are absorbed. In Fig. 3(a) a two-phase liquid with one phase absorbable (yellow) and one phase non-absorbable (green) reaches the surface of a porous solid. In Fig. 3(b)(c)(d), the absorption flux (Eqn. (13)) will first act to transfer virtual phases (from yellow to orange). Then the inner virtual phase is subject to the Darcy flux, which is an inward-direction effect trying to drag the particle inside. At this time the particle will contain different velocities between (virtual) phases, and they produce drift velocities. Roughly speaking, the absorbed phase will have a drift velocity pointing inward the solid, the non-absorbed phase will have a drift velocity pointing outward. The mixture model (Eqns. (6-8)) ensures that both concentration change and particle motion change can be adequately calculated. As a result, in Fig. 3(e) the absorbed particles will be left with more absorbed phase as it goes deeper, and the non-absorbed-phase volume fractions are transferred to the outer-region particles (Eqns. (6-7)).

5 DISCRETIZATION

In the SPH formulation, calculation of physical variables are performed through a weighted sum over neighbourhood particles. Analogue to the staggered-grid scheme, we find it convenient for some gradient and interpolation calculations to be selectively assigned to solid and fluid particles, since the solid particles can serve as reference background frame for the fluid particles nearby. Table 1 lists the model variables with the storage particle categories they belong to. In the following sections, we use $\sum_s$ for summing over nearby solid particle quantities, $\sum_f$ for summing over nearby liquid particle quantities, and $\sum_k$ for summing over k phases. Subscript f and s indicate fluid and solid, respectively.

The interpolated densities for the solid or fluid particles are computed over the same kind of particles, i.e. for a particle i, $\rho_{s,i} = \sum_j m_{s,j} W_{ij}$ and $\rho_{f,i} = \sum_j m_{f,j} W_{ij}$.

The absorbed volume rate ϕ_{sk} represents how much fluid phase k is absorbed locally at a solid particle position. It is calculated by

$$\phi_{sk} = \frac{1}{\rho_k V_{s0}} \sum_f \frac{\beta_k m_f \rho_k W_{fs}}{\rho_{fm} N_f}, \tag{15}$$

where V_{s0} denotes the rest volume of solid particle, ρ_k the rest density of phase k, $N_f = \sum_s W_{fs}$ the sum of SPH kernels between each fluid particle and its nearby solid neighbours. For any fluid particle with non-zero β_{fk}, we effectively assign its absorbed mass to nearby solid particles using an SPH-kernel weight, and Eq. (15) is the collected absorbed mass on a solid particle from nearby fluid particle contributions. Detailed derivations are given in Appendix A. The model variables $p_s^{pore}, \mathbf{q}_k, \mathbf{u}_{rk}, \mathbf{u}_{\beta k}$ are also computed on solid particles. Then we are able to interpolate $\mathbf{q}_k, \mathbf{u}_{\beta_k}$ onto fluid particles using the SPH formulation whenever needed:

$$\mathbf{u}_{\beta k,f} = \sum_s \mathbf{u}_{\beta k,s} W_{fs} / N_f \tag{16}$$

$$\mathbf{q}_{k,f} = \sum_s \mathbf{q}_{k,s} W_{fs} / N_f. \tag{17}$$

In the special case when $N_f = 0$, we simply set the left hand side to be zero.

Using the SPH formulation, on a fluid particle Eq. (14) can be discretized as:

$$\mathbf{a}_f^{cap} = \psi \sum_k (\beta_k \sum_s \frac{m_s}{\rho_s} \nabla W_{fs}). \tag{18}$$

There are several pore pressure gradients in Eqs.(1,11,13). In Eq. (1), for each solid particle s, the gradient of pore pressure is computed by:

$$\nabla p_s^{pore} = \sum_{s_j \in N_s} \frac{m_{s_j}}{\rho_{s_j}} (p_s^{pore} - p_{s_j}^{pore}) \nabla W_{ss_j}, \tag{19}$$

where N_s consists of the solid particles in s's neighbourhood.

For fluid particles, in Eq. (11), the gradient of outer fluid pore pressure is computed by

$$\nabla p_{fk}^{pore} = \sum_s \frac{m_s}{\rho_s} (p_{0k} - p_s^{pore}) \nabla W_{fs}, \tag{20}$$

where p_{0k} is defined in §4.3. For Eq. (13), we similarly have

$$\mathbf{D}_{k,f} = -K \frac{\mathbf{k_{wk}}}{\mu_k} \sum_s \frac{m_s}{\rho_s} (\alpha_{fk} + \phi_{sk})(p_{0k} - p_s^{pore}) \nabla W_{fs}. \tag{21}$$

Then we compute the absorption source term using

$$\nabla \cdot \mathbf{D}_{k,f} = \sum_s \frac{m_s}{\rho_s} \mathbf{D}_{k,f} \cdot \nabla W_{fs}. \tag{22}$$

6 IMPLEMENTATION

Algorithm 1 summarizes the overall simulation workflow. The calculation pipeline computes solid and fluid quantities in an interleaved manner, and the calculation steps are performed on all fluid or solid particles without labelling particle regions.

ALGORITHM 1: Overall Simulation Workflow

repeat
- Compute all particle densities (§5);
- Compute N_f for fluid particles (§5);
- Compute outer-fluid viscosity and $\mathbf{a}^{press}$ on fluid particles (§6.1);
- Pore pressure and Darcy flux computation on solid particles (Algorithm 2);
- Prepare equation terms on fluid particles (Algorithm 3);
- Time Integration (Algorithm 4);
- $t \leftarrow t + \Delta t$;

until *end of simulation*;

Table 1. Definition and Computation of Model Variables

Variable	Description	Storage/Calculation Location
m_s, m_f	solid/fluid particle masses	solid particle / fluid particle
α_k, β_k	virtual phase volume fraction	fluid particle
$\mathbf{u}_{mk,\alpha}, \mathbf{u}_{mk,\beta}$	drift velocities of virtual phases	fluid particle
$\mathbf{u}_m, \mathbf{u}_s$	fluid and solid particle velocities	fluid particle / solid particle
$\mathbf{u}_{rk}$	relative fluid-solid velocity of phase k	solid particle
$\mathbf{u}_{\beta k}$	world-coordinate fluid phase velocity	solid particle / fluid particle
$\tilde{\mathbf{u}}_{mk}, \tilde{\alpha}_k$	non-virtual drift velocity and volume fraction	fluid particle
ρ_{fm}, ρ_k	fluid aggregate density and phase density	fluid particle
ρ_f, ρ_s, ρ_i	interpolated density of fluid/solid/particle i	fluid particle
$\rho_{\alpha m}, \rho_{\beta m}$	outer/inner fluid mixture rest densities	fluid particle
$c_{\alpha k}, c_{\beta k}$	outer/inner mass fractions	fluid particle
$\mathbf{q}_k$	Darcy flux of phase k	solid particle / fluid particle
p_s^{pore}	pore pressure in solid	solid particle
p_{0k}	fluid phase-wise pore pressure	fluid particle
$\nabla p^{pore}, \nabla p_k^{pore}$	gradient of pore pressure (for phase k)	solid particle / fluid particle
$\mathbf{a}^{press}, \mathbf{a}^{pore}, \mathbf{a}^{cap}, \mathbf{a}^{other}$	accelerations due to related forces	fluid particle
ϵ, $\mathbf{P}$	solid strain and stress tensors	solid particle
$\mathbf{D}_k$	absorption flux	fluid particle
ϕ_{sk}	absorbed volume rate	solid particle
$\mathbf{n}$	normal vector near solid surface	fluid particle
W, N_f	SPH kernel, sum of SPH kernels	fluid particle

6.1 Outer Region Fluid Handling

Instead of using the state equation based approach as in [Ren et al. 2014; Yan et al. 2016], we use an IISPH-like scheme to compute the hydrodynamic pressure for the outer-region fluid particles, which gives better incompressibility. We adopt the same algorithm framework as [Band et al. 2018a] to compute pressure and implement two-way coupling. A series of modifications are made to support multiple-fluid porous flow simulation.

First, based on [Yan et al. 2016], the fluid viscosity is obtained as

$$\mathbf{a}_{f_i}^{visc} = \sum_f \sum_k \frac{\alpha_{f_i k}\alpha_{fk}}{\alpha_{f_i k}+\alpha_{fk}}(\mathbf{u}_{m,f}-\mathbf{u}_{m,f_i})\cdot \frac{m_f}{\rho_i\rho_f}(\mu_{mf_i}+\mu_{mf})\frac{(\mathbf{r}_f-\mathbf{r}_{f_i})\nabla W_{f_i f}}{(\mathbf{r}_f-\mathbf{r}_{f_i})^2}, \tag{23}$$

and the viscosity of the elastic solid particle can be given as:

$$\mathbf{a}_{s_i}^{visc} = \sum_s \sum_k (\mathbf{u}_s-\mathbf{u}_{m,s_i})\frac{m_s}{\rho_i\rho_s}(\mu_{ms_i}+\mu_{ms})\frac{(\mathbf{r}_s-\mathbf{r}_{s_i})\nabla W_{s_i s}}{(\mathbf{r}_s-\mathbf{r}_{s_i})^2}, \tag{24}$$

where $\mu_{mf_i}, \mu_{ms_i}, \mu_{mf}, \mu_{ms}$ are the aggregate viscosity coefficients of the particles. We set the intermediate acceleration of liquid and solid particles as $\mathbf{a}_i^* = \mathbf{a}_i^{visc}$. Here and afterwards we use i, j footnotes to indicate that the calculations apply to all neighboring fluid and solid particles. Note that for the outer region calculation, solid particles act as scene boundary for liquid pressure calculation.

We also update the rest volume of the liquid particles to the effective volume of outer liquid to exclude the absorbed fluid in the computation. At the beginning of each time step, we calculate the sum of outer-fluid volume fraction $\alpha_f = \sum_k \alpha_k$ for each fluid particle, after which its rest volume is approximated by $V_{f0} = \alpha_f h^3$. Since this volume of fluid particles near the solid varies greatly, we use the harmonic mean for better stability, so that the divergence of velocity becomes

$$\nabla \cdot \mathbf{u}_f^* = -\sum_j \frac{V_f V_j}{V_f+V_j}(\mathbf{u}_f^*-\mathbf{u}_j^*)\nabla W_{fj} \tag{25}$$

$$\nabla \cdot \mathbf{u}_s^* = -\sum_f \frac{V_f V_s}{V_f+V_s}(\mathbf{u}_s^*-\mathbf{u}_f^*)\nabla W_{sf}, \tag{26}$$

where $\mathbf{u}^*$ is the intermediate velocity in [Band et al. 2018a]. Using the intermediate velocity, [Band et al. 2018a] derived a set of linear equations $(Ap)_f = S_f$ for the particles and solve for the particle pressures p, where A is a matrix and S_f is a derived term. The same harmonic interpolation also applies to those terms in [Band et al. 2018a], e.g. for a particle i:

$$\mathbf{a}_i^{press} = -\frac{V_i}{m_i}\sum_j \frac{V_i V_j}{V_i+V_j}(p_i+p_j)\nabla W_{ij} \tag{27}$$

$$(Ap)_i = \Delta t^2 \sum_j \frac{V_i V_j}{V_i+V_j}(\mathbf{a}_i^{press}-\mathbf{a}_j^{press})\cdot\nabla W_{ij}. \tag{28}$$

We further modify the term S_f in [Band et al. 2018a] to reflect the rest volume modification:

$$S_f = \alpha_f(1+\Delta t\nabla\cdot\mathbf{u}_f^*) - \frac{V_{f0}}{V_f}. \tag{29}$$

Using the above modifications, we can solve for a pressure value for each fluid particle and solid particle (viewed as

boundary particles for outer fluid) using [Band et al. 2018a], then we can compute $\mathbf{a}^{press}$ for Eq. (8) and compute the boundary forces solid particles received from outer fluid for solid motion integration. Since $V_{f0} = \alpha_f h^3$ and V_i, V_j are its interpolation values, Eq. (27) ensures $\mathbf{a}^{press}$ vanishes for inner fluid particles even without explicit label of regions. This scheme can achieve better visual incompressibility than the original multiple fluid pressure calculation, and provide a practical solid-liquid mechanical motion solution when the liquid hits the solid.

6.2 Pore Pressure and Darcy Flux

On the solid particles, we compute the physical terms related to the Darcy's law for later computation of multiple fluid porous flow. Terms necessary for the solid motion integration are also prepared. The workflow is given in Algorithm 2.

ALGORITHM 2: Pore Pressure and Darcy Flux

Compute solid strain on solid particles (Eq. (4));
Compute pore pressure p_s^{pore} on solid particles (Eqs.(9,15));
Compute Darcy flux $\mathbf{q}_k$ on solid particles (Eqs.(1,19));
Compute $\mathbf{u}_{\beta k}$ on solid particles (§4.1);
Obtain solid stress (Eq. (5)) and boundary forces solid particle received from outer fluid (§6.1);

6.3 Fluid Term Preparation

Using the physical quantities computed on solid particles, we are able to calculate the rest terms required for fluid governing equations Eqs. (6,7,8). The workflow is given in Algorithm 3.

ALGORITHM 3: Fluid Term Preparation

Compute $\mathbf{a}^{pore}$ on fluid particles (Eqs.(10,16));
Compute drift velocities (Eqs.(11,12,17,20));
Compute absorption source term $\nabla \cdot \mathbf{D}_k$ (Eqs.(13,21,22));
Compute $\mathbf{a}^{cap}$ (Eqs.(14,18));

6.4 Time Integration

Finally, we perform time integration for the solid and fluid motions. The workflow is given in Algorithm 4. The integration of solid equations can be solved explicitly or implicitly subject to the solid model choice. The integration of governing equations for fluid particles is in a semi-implicit manner. That is, we solve for $\mathbf{a}^{press}$ as in §6.1, then explicitly calculate other terms in Eqs.(6,7,8), with standard SPH particle advancing scheme using $\mathbf{u}_m$ computed from the momentum equation. Thanks to the mixture model, the virtual volume fraction changes within each particle are automatically handled by integration of the continuity equations, where the volume fraction changes rely on local divergences, and no explicit mass or volume fraction advection is needed. However, the explicit integration is still subject to CFL conditions that limits the time step size, a detailed discussion can be found in [Ren et al. 2014]. It is noted that although we adopt [Peer et al. 2018] for the solid model by default, our algorithm framework has the flexibility to allow for other kinds of solid physical models. An example is given in §7 Fig. 11, where we use the solid model in [Yang et al. 2017] and simulates a two-phase sand-water flow. We ensure $\sum_k(\alpha_k + \beta_k) = 1$ in a similar way with [Ren et al. 2014], i.e. first setting negative values of α_k, β_k to zero, and then re-scale them so that their sum equals 1.

ALGORITHM 4: Time Integration

```
Integrate solid particle motion using [Peer et al. 2018];
Integrate Eqs.(6,7,8);
for each fluid particle do
    Ensure Σ_k(α_k + β_k) = 1 (§6.4);
    if (N_f == 0) then
        α_k += β_k;
        β_k = 0;
    end
end
```

6.5 Parameter Discussion

The typical model settings for our simulation examples are listed Table 2. Most parameters (e.g. $\rho_k, \mu_k, \nu, \lambda, \eta, B, \tau, \sigma, \sigma', \psi, e$) are set according to the physical properties of the fluids and porous solid present in the simulation. Besides these, the parameters φ, τ' play a similar role to τ from [Ren et al. 2014], and in our simulation we choose their values to set the related term at approximately the same order with other terms. The parameter μ_k is set to be the same among phases. Certain coefficients can be set to zero or near-zero to turn-off the related effects such as expansion of solid due to absorption (η), capillary force (ψ) and overall absorption (K).

A few parameters directly link to the porous behaviour and deserve further discussions, which include $p_0, p_{0k}, \mathbf{k}_{wk}, K$. The permeability $\mathbf{k}_{wk}$ controls how fast the absorbed fluid moves within the porous solid, and we assume the solid is homogeneous and set it as a scalar value. From Eq. (13), the absorption rate is proportional to $\mathbf{k}_{wk}K$, which controls how fast fluid enters the porous solid. The parameters p_0, p_{0k} controls the stability state of how much fluid can enter the porous solid in total, and they also influence the gradient of pressure, thereby affecting fluid absorption and transport speed in solid. Higher $p_{0k} - p_0$ will usually increase the absorption speed, fluid transport speed in solid and final absorbed fluid amount.

We demonstrate the effects of these parameters in Fig. 4. In the first row, the first column shows a reference simulation results. In the second column, we use a larger absorption coefficient K, and relatively more liquid is absorbed during the same time. In the third column, we raise k_{wk} but keeps $k_{wk}K$ the same, the fluid transport speed within the solid is largely increased while the colour is slightly lighter due to less dense fluid concentration. The fourth column shows a result with higher p_{0k}, where fluid is easier to enter solid

Table 2. Model Parameters

	Typical Value	Description
ρ_k	600 kg/m^3	density
μ_k	0.35-1 $Pa \cdot s$	viscosity coefficient
ν	$1e^4$-$2e^4$ Pa	Lamé parameter
λ	$0.5e^4$-$1.2e^4$ Pa	Lamé parameter
η	$7.5e^{-4}$	solid constant
ψ	1-4 m^2/s^2	capillary strength
e	0.6	porosity
k_{wk}	$1e^{-8}$-$5e^{-7}$ m^2s/Pa	permeability
K	0.75-2	absorption ratio
B	$4.90e^4$ Pa	Biot's ratio constant
τ	$3e^{-6}$ $m/(Pa \cdot s)$	outer/inner drift velocity weight
τ'	$1e^{-4}$ $m/(Pa \cdot s)$	inner drift velocity weight
σ	$1e^{-3}$ m^2/s	outer drift velocity weight
σ'	$2e^{-3}$ m^2/s	inner drift velocity weight
φ	$3e^{-6}$ $m/(Pa \cdot s)$	outer drift velocity weight
p_0	$5e^4$ Pa	solid rest pore pressure
p_{0k}	$2.5e^4$ Pa	outer liquid pore pressure

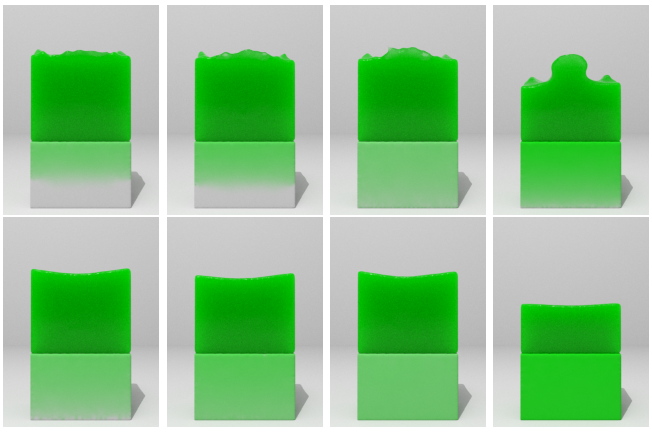

Fig. 4. Effects of parameters linking to porous behaviors. From left to right: standard, higher absorption rate, higher permeability, higher p_{0k}. Higher absorption rate makes the fluid enter the solid faster. Higher permeability leads to higher fluid transport speed within solid, and results in a lighter colour at beginning. Higher p_{0k} increases both fluid absorption and transport speeds, and results in a deeper colour in the end.

due to higher outer pore pressure setting. The second row shows the later result in the same simulations. On top of the solid, there are non-absorbed fluid left out. The first and third column have the largest non-absorbed amount followed by the second column, whose absorption rate is higher but does not influence the final absorption amount. The solid colours in the first three columns of the second row are also almost the same. On the contrary, the fourth column shows obviously less amount of non-absorbed fluid and denser concentration of inner fluid.

Table 3. Performance Data

	Liquid Phases	Liquid Particles	Solid Particles	runtime (second/step)
Example 1	1	402,000	247,000	0.36
Example 2	2	980,000	120,000	0.47
Example 3	1	1,683,000	41,000	0.40
Example 4	2	1,091,000	524,000	0.42
Example 5	3	693,000	448,000	0.38
Example 6	3	1,055,000	2,098,000	0.84
Example 7	1	178,000	133,000	0.09

7 RESULTS

We implemented the proposed approach on an Nvidia GeForce GTX 1080Ti GPU. The performances of the simulations in this section are recorded in Table 3. In the experiments, the particle mass and the width of the scene are typically set to $0.2g$ and between $0.1m - 1m$. We generally choose a fixed time step that is below the CFL time steps and ensures the solid solver and outer-fluid solver are both stable. Each frame in the supplemental video (30 frames per second) contains 10 steps.

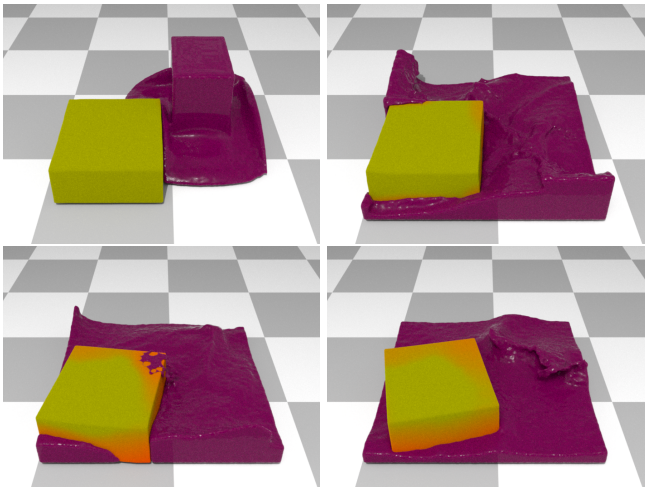

Fig. 5. Single fluid porous flow. The regions where liquid is absorbed are rendered in orange colour.

Example 1 (Fig. 5) shows a porous block absorbing a single fluid. When the flow wave reaches the solid surface, it causes distortion of the solid body and the flow is bounced back. At the same time some liquid gets absorbed into the porous material, leaving visual traces when the bulk liquid drops back. In the bottom-left we can observe lower wet orange regions of the solid expand in volume showing poroelasticity effect. Since no particle deletion or insertion is needed, our approach automatically guarantees the mass conservation throughout the simulation.

Example 2 (Fig. 6) shows a porous solid in a two-phase flow. The two fluid phases are mixed as $1:1$ volume fraction,

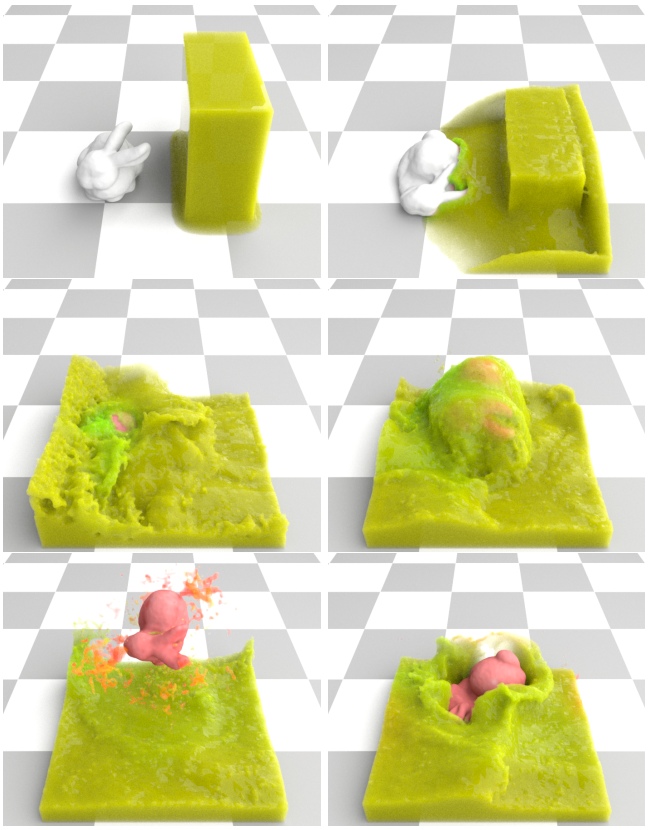

Fig. 6. A two-phase mixture (red and green) interacts with a porous rabbit. Initially, the mixture turns into green around the porous rabbit (first row), because only the red phase can be absorbed into the porous solid. Then, the rabbit is lifted out of the liquid mixture (second row) and squeezed (third row), causing some red phase to come out and remix into the liquid.

but only the red liquid can be absorbed by the porous solid. Using the proposed virtual phase concept, complex coupling of different governing equations in inner and outer regions is resolved. Consistent mass and momentum transport is achieved without particle splitting, with only red phase entering the solid and the green phase being left outside. During the simulation the rabbit is squeezed, pushing some red liquid out from the solid. The capillary effect at porous surface prevents the red liquid from free escape.

Example 3 (Fig. 7) demonstrates that the solid-particle properties can be influenced by absorbing the liquid. Initially, the porous dumbbell has uniform density and is lighter than the liquid. Then, the yellow side becomes heavier after absorbing liquid. As absorbed fluid amount increases, it gradually changes colour to blue and drags the whole dumbbell into the tank. To achieve this effect, we only need to adjust the mass for solid particles so that they increase with the ϕ_{sk} value, i.e. adding the absorbed liquid mass onto the solid mass.

In Example 4 (Fig. 8), two fluid phases pass through a perforated material separately. The two fluid phases are absorbed differently by the solid, and as a result the red phase

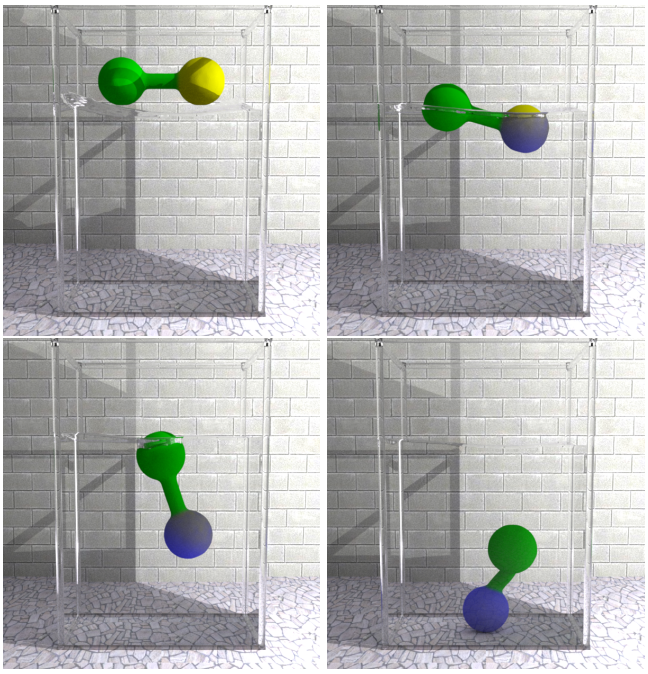

Fig. 7. Solid property changes with liquid absorption. After absorbing liquid, the yellow end becomes heavier and drags the dumbbell to sink.

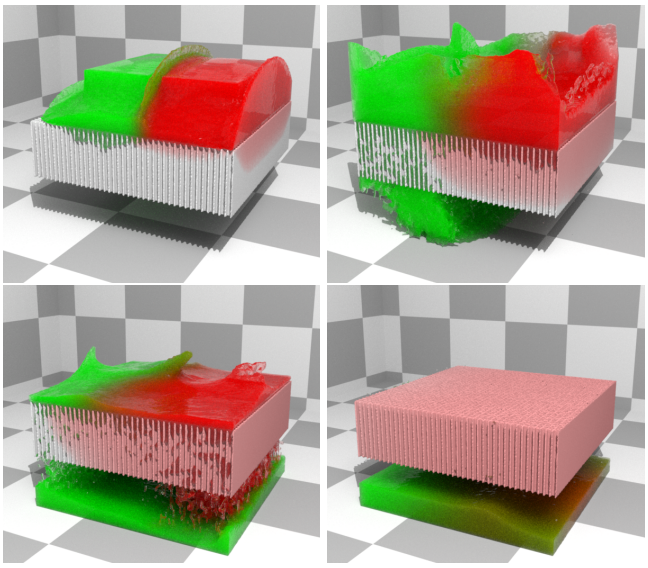

Fig. 8. Two fluids pass through a perforated material. The less-absorbed green phase passes the solid region faster, leaving the red phase behind.

is largely trapped in the solid while the less-absorbed green phase falls almost freely through the perforated material.

In Example 5 (Fig. 1) a three-phase mixture is poured onto a stack of three porous solids, where each porous solid can

only absorb one specific liquid phase. There are smaller vertical holes in the filter layers (Fig. 9) to let the non-absorbed phases pass through, which are not shown in the final rendering. The radius of a hole equals to h, the smooth radius. There are about 500 holes in the cross section of the layers. The liquid mixture first builds up on the top of solid stack due to the resistance from the porous solids. Then, as each liquid phase passes through and gets absorbed by the porous solid, both the liquid mixture and the porous solids change colour. Finally, the liquid at the bottom of container shows a blueish colour, which corresponds to the less absorbed phases.

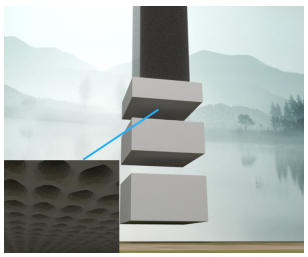

Fig. 9. Cutout view of solid layer setting in Fig.1.

In Example 6 (Fig. 10) several contacting solid regions have different absorption abilities for the fluid phases. The left of the solid only absorbs green fluid; in the middle, an S-shaped region only absorbs blue fluid and the rest only absorbs red fluid. The right of the solid absorbs both blue and green fluids but with different permeability, and the blue fluid moves faster within the solid leaving the green fluid behind. In this example, we only adjust the physical porous parameters within each solid region without explicitly labelling the regions in the simulation. The simulation result shows correct behaviour when different solid regions are in contact and the behaviour of fluid unmixing in solid is also achieved.

In Example 7 (Fig. 11) we demonstrate our approach can also cover sand-like porous materials. The time step size is 5 times smaller for this case for stability of the solid solver, with 25 steps in one frame in the supplemental video. The solid model of [Yang et al. 2017] is adopted in this example. The top and middle rows show our result with larger and smaller wet sand cohesion. In the bottom row, we show a result of [Yang et al. 2017] under the smaller wet sand cohesion. The comparable result shows that our approach is able to cover sand-like porous materials as well.

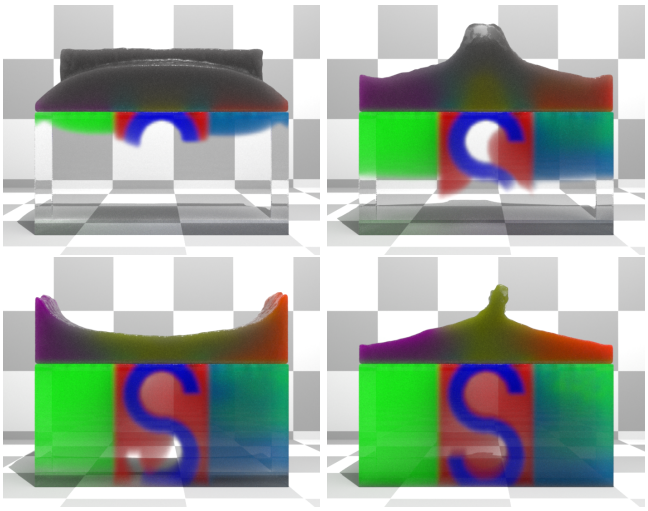

Fig. 10. Porous behaviour in multiple contacting solid regions. The solid comprises three parts: the left part only absorbs green fluid, the S-shaped region only absorbs blue fluid with the remaining middle part absorbing only red fluid, the right part absorbs both blue and green fluids with different permeability such that the blue fluid moves faster leaving the green fluid behind.

8 CONCLUSION

We present an SPH-based simulation scheme for multiple-fluid liquid flow interacting with sponge-like porous materials. By introducing virtual phases, the SPH fluid particles are universally handled without deleting or splitting particles at the solid surface. Our approach is flexible on solid model choices and ensures physically consistent mass and momentum transport using the mixture model.

Our current framework does not consider degenerate cases, such as very thin layers of fluid, where there are serious neighborhood particle deficiency and the SPH formulation will give erroneous calculations. Stray particles containing both absorbed and non-absorbed phases might get stuck on surface but will behave normal again when they meet bulk fluid. The simplification made in the proposed approach also causes some limitations. Darcy's law does not model free flow inside the porous material, and is less suitable for materials with larger voids or fractures. In addition, assigning a constant outer-region pore pressure for each phase during solid-surface absorption is a simple and effective treatment, but may not be enough for certain cases where complex relative absorption tendency variations between multiple solid and fluid phases exist. A possible solution involves decoupling the phase-wise pore pressures in the solid, which we would like to investigate in the future. The volume fraction correction in Algorithm 4 is explicit and does not take consideration of its influence to the momentum calculation, which may produce errors in mass calculation under very large time steps. We would like to investigate efficient combined integration methods of the continuity and momentum equations that strictly ensures phase-mass conservation in the future.

ACKNOWLEDGMENTS

This work was supported by the National Key R&D Program of China under Grant 2017YFB1002701. We thank the anonymous reviewers for suggestions. We also appreciate the helpful discussions with Xiao Yan and Yuntao Jiang.

REFERENCES

Nadir Akinci, Markus Ihmsen, Gizem Akinci, Barbara Solenthaler, and Matthias Teschner. 2012. Versatile Rigid-Fluid Coupling for Incompressible SPH. *ACM Trans. Graph.* 31, 4, Article 62 (July 2012), 8 pages.

Abdelraheem M. Aly and Z.A.S. Raizah. 2018. Incompressible smoothed particle hydrodynamics (ISPH) method for natural convection in a

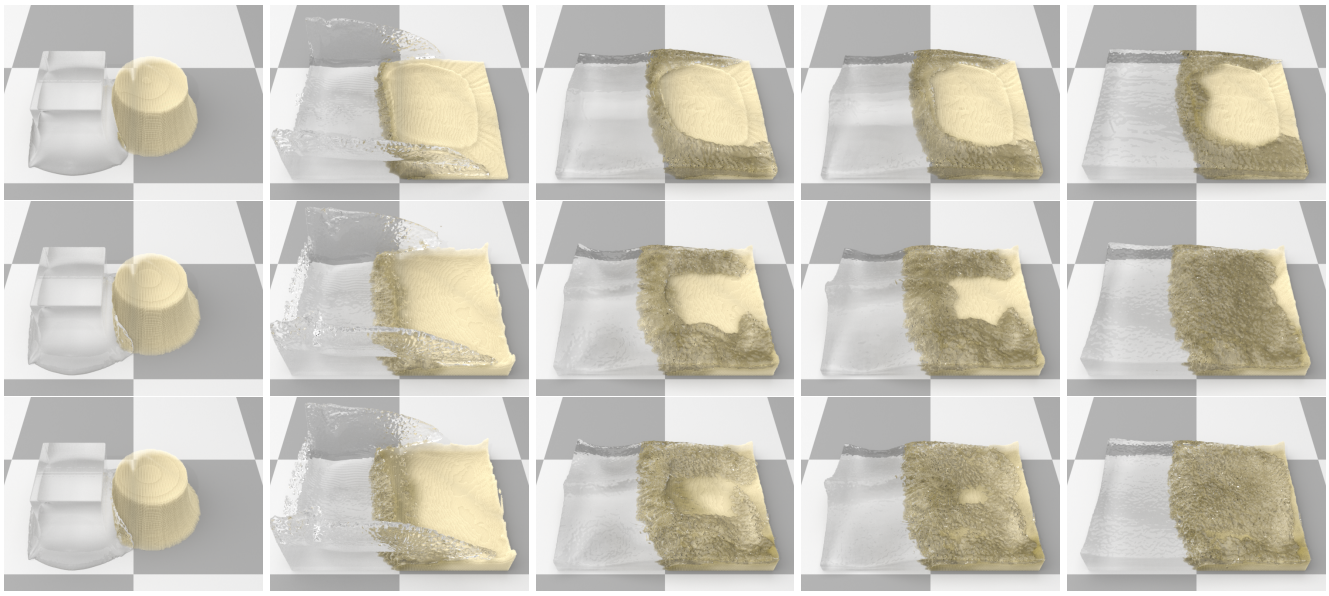

Fig. 11. Changing the solid model for a sand-water two-phase mixture. The solid model of [Yang et al. 2017] is adopted. Top row and middle row: our result with larger and smaller wet sand cohesion. Bottom row: result of [Yang et al. 2017] under the smaller wet sand cohesion. The comparable result shows that our approach is able to cover sand-like porous materials as well.

nanofluid-filled cavity including rotating solid structures. *International Journal of Mechanical Sciences* 146-147 (2018), 125 – 140.

Seungho Baek, Kiwon Um, and JungHyun Han. 2015. Muddy water animation with different details. *Computer Animation and Virtual Worlds* 26, 3-4 (2015), 347–355.

Stefan Band, Christoph Gissler, Markus Ihmsen, Jens Cornelis, Andreas Peer, and Matthias Teschner. 2018a. Pressure Boundaries for Implicit Incompressible SPH. *ACM Trans. Graph.* 37, 2, Article 14 (Feb. 2018), 11 pages.

Stefan Band, Christoph Gissler, Andreas Peer, and Matthias Teschner. 2018b. MLS pressure boundaries for divergence-free and viscous SPH fluids. *Computers & Graphics* 76 (2018), 37 – 46.

Kai Bao, Xiaolong Wu, Hui Zhang, and Enhua Wu. 2010. Volume fraction based miscible and immiscible fluid animation. *Computer Animation and Virtual Worlds* 21, 3-4 (2010), 401–410.

Markus Becker and Matthias Teschner. 2007a. Weakly Compressible SPH for Free Surface Flows. *Proceedings of the 2007 ACM SIGGRAPH/Eurographics Symposium on Computer Animation* 9, 209–217.

Markus Becker and Matthias Teschner. 2007b. Weakly compressible SPH for free surface flows. In *Proceedings of the 2007 ACM SIGGRAPH/Eurographics symposium on Computer animation*. Eurographics Association, 209–217.

Jan Bender and Dan Koschier. 2016. Divergence-Free SPH for Incompressible and Viscous Fluids. *IEEE Transactions on Visualization and Computer Graphics* 23 (06 2016), 1–1.

J. Bender, T. Kugelstadt, M. Weiler, and D. Koschier. 2020. Implicit Frictional Boundary Handling for SPH. *IEEE Transactions on Visualization and Computer Graphics* 26, 10 (2020), 2982–2993.

Stefano Berrone, Sandra Pieraccini, and Stefano Scialo. 2017. Flow simulations in porous media with immersed intersecting fractures. *JOURNAL OF COMPUTATIONAL PHYSICS* 345 (SEP 15 2017), 768–791. https://doi.org/{10.1016/j.jcp.2017.05.049}

Henry Philibert Gaspard Darcy. 1856. *Les Fontaines publiques de la ville de Dijon. Exposition et application des principes à suivre et des formules à employer dans les questions de distribution d'eau, etc.* V. Dalamont.

E. Detournay and Alexander H.-D. Cheng. 1993. 5 - Fundamentals of Poroelasticity. In *Analysis and Design Methods*, CHARLES FAIRHURST (Ed.). Pergamon, Oxford, 113 – 171.

Mengyuan Ding, Xuchen Han, Stephanie Wang, Theodore F. Gast, and Joseph M. Teran. 2019. A Thermomechanical Material Point Method for Baking and Cooking. *ACM Trans. Graph.* 38, 6, Article 192 (Nov. 2019), 14 pages.

Yun Fei, Christopher Batty, Eitan Grinspun, and Changxi Zheng. 2018. A multi-scale model for simulating liquid-fabric interactions. *ACM Transactions on Graphics* 37 (07 2018), 1–16.

Yun (Raymond) Fei, Henrique Teles Maia, Christopher Batty, Changxi Zheng, and Eitan Grinspun. 2017. A Multi-Scale Model for Simulating Liquid-Hair Interactions. *ACM Trans. Graph.* 36, 4, Article 56 (July 2017), 17 pages.

Ming Gao, Andre Pradhana, Xuchen Han, Qi Guo, Grant Kot, Eftychios Sifakis, and Chenfanfu Jiang. 2018. Animating Fluid Sediment Mixture in Particle-Laden Flows. *ACM Trans. Graph.* 37, 4, Article 149 (July 2018), 11 pages.

Christoph Gissler, Andreas Peer, Stefan Band, Jan Bender, and Matthias Teschner. 2019. Interlinked SPH Pressure Solvers for Strong Fluid-Rigid Coupling. *ACM Trans. Graph.* 38, 1, Article 5 (Jan. 2019), 13 pages.

R Hilfer. 2006. Macroscopic capillarity and hysteresis for flow in porous media. *Physical review. E, Statistical, nonlinear, and soft matter physics* 73 (02 2006), 016307.

Jeong-Mo Hong and Chang-Hun Kim. 2005. Discontinuous Fluids. *ACM Trans. Graph.* 24, 3 (July 2005), 915–920.

Markus Huber, Simon Pabst, and Wolfgang Straßer. 2011. Wet Cloth Simulation. In *ACM SIGGRAPH 2011 Posters* (Vancouver, British Columbia, Canada) *(SIGGRAPH '11)*. Association for Computing Machinery, New York, NY, USA, Article 10, 1 pages.

Markus Ihmsen, Jens Cornelis, Barbara Solenthaler, Christopher Horvath, and Matthias Teschner. 2014a. Implicit Incompressible SPH. *IEEE Transactions on Visualization and Computer Graphics* 20, 3 (March 2014), 426–435.

Markus Ihmsen, Jens Orthmann, Barbara Solenthaler, Andreas Kolb, and Matthias Teschner. 2014b. SPH Fluids in Computer Graphics. In *Eurographics 2014 - State of the Art Reports*, Sylvain Lefebvre and Michela Spagnuolo (Eds.). The Eurographics Association.

Yi Jin, Xiang Li, Mengyu Zhao, Xianhe Liu, and Hui Li. 2017. A mathematical model of fluid flow in tight porous media based on fractal assumptions. *International journal of heat and mass transfer* 108 (2017), 1078–1088.

Nahyup Kang, Jinho Park, Junyong Noh, and Sung Yong Shin. 2010. A hybrid approach to multiple fluid simulation using volume fractions. In *Computer Graphics Forum*, Vol. 29. Wiley Online Library, 685–694.

Byungmoon Kim. 2010. Multi-phase Fluid Simulations Using Regional Level Sets. *ACM Trans. Graph.* 29, 6, Article 175 (Dec. 2010),

8 pages.
Dan Koschier and Jan Bender. 2017. Density Maps for Improved SPH Boundary Handling. In *Proceedings of the ACM SIGGRAPH / Eurographics Symposium on Computer Animation* (Los Angeles, California) *(SCA '17)*. Association for Computing Machinery, New York, NY, USA, Article 1, 10 pages.
Dan Koschier, J. Bender, B. Solenthaler, and Matthias Teschner. 2019. Smoothed Particle Hydrodynamics Techniques for the Physics Based Simulation of Fluids and Solids. In *Eurographics*.
Toon Lenaerts, Bart Adams, and Philip Dutre. 2008. Porous flow in particle-based fluid simulations. *ACM TRANSACTIONS ON GRAPHICS* 27, 3 (AUG 2008). ACM SIGGRAPH Conference 2008, Singapore, SINGAPORE, AUG 11-15, 2008.
Toon Lenaerts and Philip Dutre. 2009. Mixing Fluids and Granular Materials. *Computer Graphics Forum* 28, 2 (2009), 213–218.
Wei-Chin Lin. 2015. Boundary handling and porous flow for fluid-hair interactions. *COMPUTERS & GRAPHICS-UK* 52 (NOV 2015), 33–42. https://doi.org/{10.1016/j.cag.2015.06.005} 11th European Conference on Visual Media Production (CVMP), London, ENGLAND, NOV 13-14, 2014.
Frank Losasso, Tamar Shinar, Andrew Selle, and Ronald Fedkiw. 2006. Multiple Interacting Liquids. *ACM Trans. Graph.* 25, 3 (July 2006), 812–819.
Miles Macklin and Matthias Müller. 2013. Position Based Fluids. *ACM Trans. Graph.* 32, 4, Article 104 (July 2013), 12 pages.
J.J. Monaghan. 1994. Simulating Free Surface Flows with SPH. *J. Comput. Phys.* 110, 2 (1994), 399 – 406.
Matthias Müller, David Charypar, and Markus H Gross. 2003. Particle-based fluid simulation for interactive applications.. In *Symposium on Computer animation*. 154–159.
Kentaro Nagasawa, Takayuki Suzuki, Ryohei Seto, Masato Okada, and Yonghao Yue. 2019. Mixing Sauces: A Viscosity Blending Model for Shear Thinning Fluids. *ACM Trans. Graph.* 38, 4, Article 95 (July 2019), 17 pages.
Michael B. Nielsen and Ole Osterby. 2013. A Two-continua Approach to Eulerian Simulation of Water Spray. *ACM Trans. Graph.* 32, 4, Article 67 (July 2013), 10 pages.
S. Patkar and P. Chaudhuri. 2013. Wetting of Porous Solids. *IEEE Transactions on Visualization and Computer Graphics* 19, 9 (2013), 1592–1604.
Andreas Peer, Christoph Gissler, Stefan Band, and Matthias Teschner. 2018. An Implicit SPH Formulation for Incompressible Linearly Elastic Solids. *Computer Graphics Forum* 37, 6 (2018), 135–148.
Bo Ren, Chenfeng Li, Xiao Yan, Ming C. Lin, Javier Bonet, and Shi-Min Hu. 2014. Multiple-Fluid SPH Simulation Using a Mixture Model. *ACM Trans. Graph.* 33, 5, Article 171 (Sept. 2014), 11 pages.
Bo Ren, Xu-Yun Yang, Ming Lin, Nils Thuerey, Matthias Teschner, and Chen-Feng Li. 2018a. Visual Simulation of Multiple Fluids in Computer Graphics: A State-of-the-Art Report. *Journal of Computer Science and Technology* 33 (05 2018), 431–451.
Bo Ren, Tailing Yuan, Chenfeng Li, Kun Xu, and Shi-min Hu. 2018b. Real-Time High-Fidelity Surface Flow Simulation. *IEEE Transactions on Visualization and Computer Graphics* 24, 8 (2018), 2411–2423.
Witawat Rungjiratananon, Zoltan Szego, Yoshihiro Kanamori, and Tomoyuki Nishita. 2008. Real-time Animation of Sand-Water Interaction. *Computer Graphics Forum* 27, 7 (2008), 1887–1893.
B. Solenthaler and R. Pajarola. 2009. Predictive-corrective Incompressible SPH. *ACM Trans. Graph.* 28, 3, Article 40 (July 2009), 6 pages.
Andre Pradhana Tampubolon, Theodore Gast, Gergely Klár, Chuyuan Fu, Joseph Teran, Chenfanfu Jiang, and Ken Museth. 2017. Multi-Species Simulation of Porous Sand and Water Mixtures. *ACM Trans. Graph.* 36, 4, Article 105 (July 2017), 11 pages.
Kiwon Um, Tae-Yong Kim, Youngdon Kwon, and JungHyun Han. 2013. Porous deformable shell simulation with surface water flow and saturation. *Computer Animation and Virtual Worlds* 24, 3-4 (2013), 247–254.
Yu-Shu Wu, Lehua Pan, and Karsten Pruess. 2004. A physically based approach for modeling multiphase fracture–matrix interaction in fractured porous media. *Advances in Water Resources* 27, 9 (2004), 875–887.
Xiao Yan, Yun-Tao Jiang, Chen-Feng Li, Ralph R. Martin, and Shi-Min Hu. 2016. Multiphase SPH Simulation for Interactive Fluids and Solids. *ACM Trans. Graph.* 35, 4, Article 79 (July 2016), 11 pages.
Xiao Yan, C-F Li, X-S Chen, and S-M Hu. 2018. MPM simulation of interacting fluids and solids. 37, 8 (2018), 183–193.
Tao Yang, Jian Chang, Ming C. Lin, Ralph R. Martin, Jian J. Zhang, and Shi-Min Hu. 2017. A Unified Particle System Framework for Multi-Phase, Multi-Material Visual Simulations. *ACM Trans. Graph.* 36, 6, Article 224 (Nov. 2017), 13 pages.
Tao Yang, Jian Chang, Bo Ren, Ming C. Lin, Jian Jun Zhang, and Shi-Min Hu. 2015. Fast Multiple-fluid Simulation Using Helmholtz Free Energy. *ACM Trans. Graph.* 34, 6, Article 201 (Oct. 2015), 11 pages.
Yi Zheng, Lei Ma, Yanyun Chen, Guangzheng Fei, Bin Sheng, and Enhua Wu. 2020. Simulation of multi-solvent stains on textile. *The Visual Computer* (07 2020).

A ABSORBED VOLUME RATE

To compute the absorbed volume rate, we set m_{sk} as the phase k's absorbed mass on solid particle s and m_{fk} as the phase k's absorbed mass on fluid particle. First, the following relations hold for m_{fk}:

$$m_{fk} = \frac{\beta_{fk}\rho_{fk}}{\rho_{fm}} m_f. \tag{30}$$

Distributing this mass to nearby solid particles using SPH kernel as weight gives:

$$m_{sk} = \sum_f \frac{m_{fk} W_{fs}}{N_f}. \tag{31}$$

The above two equations can be merged and simplified to

$$m_{sk} = \sum_f \frac{\beta_{fk}\rho_{fk} m_f W_{fs}}{\rho_{fm} N_f}. \tag{32}$$

Then we can obtain

$$\beta_{sk} = \frac{m_{sk}}{\rho_k V_{s0}}, \tag{33}$$

where V_{s0} is the rest volume of the solid particle given in the initialization.

B PORE ACCELERATION

For each fluid particle, each phase has individual phase velocity and fluid particle moves according to the mixture velocity $\mathbf{u}_m$. The mixture velocity is computed by $\mathbf{u}_m = \frac{1}{\rho_m}\sum_k \rho_k(\alpha_k \mathbf{u}_{\alpha k} + \beta_k \mathbf{u}_{\beta k})$, and the mixture density is computed by $\rho_m = \sum_k(\alpha_k + \beta_k)\rho_k$.

We first equate the impulse of desired inner forces to the momentum change of inner mixture:

$$\sum_k \rho_k \beta_k V \mathbf{a}_k^* \Delta t = \sum_k \rho_k \beta_k V \mathbf{u}_{\beta k} - \rho_{\beta m} \sum_k \beta_k V \mathbf{u}_m, \tag{34}$$

where $\rho_{\beta m} = \sum_k \frac{\beta_k \rho_k}{\sum_{k'} \beta_{k'}}$. A solution to this equation is given by:

$$\mathbf{a}_k^* = \frac{\rho_k \mathbf{u}_{\beta k} - \rho_{\beta m}\mathbf{u}_m}{\rho_k \Delta t}. \tag{35}$$

Then, assuming

$$\rho_{fm} V \mathbf{a}^{pore} = \sum_k \rho_k \beta_k V \mathbf{a}_k^*, \tag{36}$$

we can obtain the $\mathbf{a}^{pore}$ term in Eq. (10).